JACS
JOURNAL OF THE AMERICAN CHEMICAL SOCIETY
pubs.acs.org/JACS
Article

A Resilient Platform for the Discrete Functionalization of Gold Surfaces Based on N-Heterocyclic Carbene Self-Assembled Monolayers

Joseph M. Palasz,[#] Zhuoran Long,[#] Jinhui Meng, Pablo E. Videla, H. Ray Kelly, Tianquan Lian, Victor S. Batista, and Clifford P. Kubiak*

Cite This: J. Am. Chem. Soc. 2024, 146, 10489−10497
Read Online
ACCESS | Metrics & More | Article Recommendations | Supporting Information

ABSTRACT: We describe the synthesis and characterization of a versatile platform for gold functionalization, based on self-assembled monolayers (SAMs) of distal-pyridine-functionalized N-heterocyclic carbenes (NHC) derived from bis(NHC) Au(I) complexes. The SAMs are characterized using polarization-modulation infrared reflectance-absorption spectroscopy, surface-enhanced Raman spectroscopy, and X-ray photoelectron spectroscopy. The binding mode is examined computationally using density functional theory, including calculations of vibrational spectra and direct comparisons to the experimental spectroscopic signatures of the monolayers. Our joint computational and experimental analyses provide structural information about the SAM binding geometries under ambient conditions. Additionally, we examine the reactivity of the pyridine-functionalized SAMs toward H_2SO_4 and $W(CO)_5(THF)$ and verify the preservation of the introduced functionality at the interface. Our results demonstrate the versatility of N-heterocyclic carbenes as robust platforms for on-surface acid−base and ligand exchange reactions.

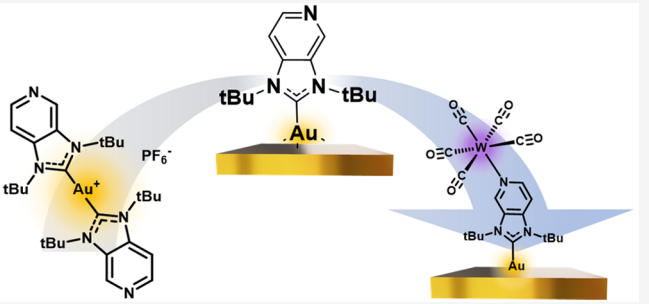

INTRODUCTION

Self-assembled monolayers (SAMs) have been a vital platform for understanding the nature of chemistry at interfaces. The ability to attach molecules onto surfaces using discrete chemical reactions, introducing specific chemical functionalities to heterogeneous interfaces, has proven useful in a variety of contexts, including electrochemistry, biopolymer synthesis, electronics, and even household hydrophobic coatings. Thiol SAMs on gold surfaces have received significant attention due to the well-behaved nature of Au(111) surfaces and the benchtop stability of the thiol and disulfide precursors.[1] The material properties of gold surfaces also enable a wide array of surface-sensitive spectroscopic and electrochemical characterization techniques. While thiol−gold bonds are reasonably strong, thiol SAMs are still sensitive to a variety of chemical conditions such as extreme pH, elevated temperature, or cathodic or anodic electrochemical bias, limiting the scope of applications.[2]

Crudden and co-workers have recently investigated N-heterocyclic carbenes (NHCs), which form stable attachments to gold and other metals, as well as semimetal surfaces.[3−5] These monolayers display dramatically improved stability at extreme pH, at elevated temperatures, in coordinating solvents,[5] and across wide electrochemical biases.[6] While NHC-derived monolayers show impressive stability, they have yet to become as widespread as their thiol-derived counterparts due, in part, to the conditions necessary to prepare the carbene precursors. This interferes with the desired ability to synthesize highly functionalized SAM possessing groups, which may react with both a free carbene and the strong bases used to prepare them.

Some work has been done exploring "masked carbene" species such as imidazolium hydrogen carbonate salts, which can form NHC monolayers under more facile conditions.[7] This route has proven widely successful for thermally evaporating carbene monolayers under UHV conditions for STM studies[4,8] as well as under ambient conditions.[7,9] In our hands, we experienced deleterious reactivity with these masked carbenes with various functionalities we desired to anchor to gold surfaces. It has been shown that masked carbenes derived from imidazolium bicarbonate salts can still exhibit the same reactivity as a free carbene.[10] We were interested in pursuing surface deposition routes that can protect the surface reactivity of the carbene in a way that enables the introduction of more

Received: December 13, 2023
Revised: March 29, 2024
Accepted: April 1, 2024
Published: April 8, 2024

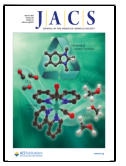

https://doi.org/10.1021/jacs.3c14113
J. Am. Chem. Soc. 2024, 146, 10489−10497

Scheme 1. Schematic Showing Previous Work Studying Functionalized Monolayers Based on Benzimidazolium-Derived N-Heterocyclic Carbenes and the Surface Functionalization Strategy, Structure, and Reactivity of the Imidazo-Pyridine-Derived Monolayers Studied in This Work

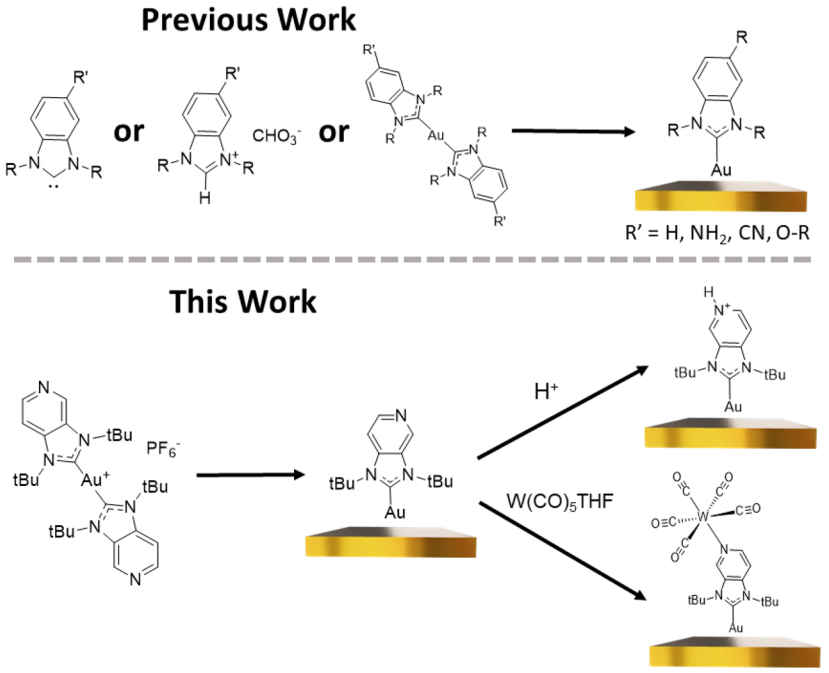

sensitive chemical functionalities that would otherwise react with the intended surface-anchoring carbene moiety.

The first report of NHCs attached to Au surfaces was by Tilley et al., where they prepared nanoparticles from the reduction of a molecular NHC-gold complex.[11] Doud et al. recently published a study of the single-molecule conductance of an NHC-based molecule where the junction was formed by reducing an (NHC)AuCl complex in situ at the molecular junction.[12] Similarly, recent work with metallic nanoparticles found that molecular NHC metal complexes can act to transfer NHCs to nanoparticle surfaces[13] and can provide a great deal of longevity to gold nanostructures.[14,15] NHC-functionalized gold nanoparticles have also been prepared directly from imidazolium aurate salts.[16]

Here, we explore the use of homoleptic imidazopyridine-based bis(NHC)Au(I) cations as facile precursors to pyridine-functionalized SAMs on bulk gold surfaces (Scheme 1). This approach leverages the high stability of the Au−NHC bond to act as a protecting group for the surface attachment moiety, allowing for sequential chemical modifications that introduce sensitive chemical functionalities such as organometallic species. We examine the binding modes and stability of these monolayers using polarization-modulation infrared reflection absorption spectroscopy (PM-IRRAS), surface-enhanced Raman spectroscopy (SERS) paired with atomistic simulations of the gold−carbene interface, X-ray photoelectron spectroscopy (XPS), and computational modeling at the density functional theory (DFT) level. To our knowledge, this is the first example of an NHC-based monolayer featuring a distal pyridine functional group, so we also demonstrate the reactivity of these pyridine-functionalized monolayers as both Bronsted and Lewis bases.

EXPERIMENTAL METHODS

All chemicals were used as received, unless otherwise noted. Reactions conducted under an inert atmosphere were handled either using the Schlenk technique or in a Vacuum Atmospheres Nexus One glovebox operating under a nitrogen atmosphere. All solvents used for synthesis were dried over an alumina column under an argon atmosphere on a Grubbs-style solvent purification system. Solutions of $W(CO)_5THF$ were prepared by UV photolysis of $W(CO)_6$ in degassed THF solution.[17] Synthesis of the $[PyNHC\text{-}H]PF_6$ precursor followed previously reported protocols substituting *tert*-butylamine in the aminative coupling.[18] The bis-NHC gold complex $[(PyNHC)_2Au]\text{-}PF_6$ was prepared by previously reported methods substituting imidazolium precursors for $[PyNHC\text{-}H]PF_6$.[19] Full synthetic details are provided in the Supporting Information (SI). Gold slides for PM-IRRAS measurements were prepared by e-beam evaporation or purchased from Angstrom Engineering for the preparation of surface-enhanced Raman substrates.

Preparation of Au SERS-Active Surface. The SERS-active Au surface was prepared by drop-casting the synthesized Au nanoparticles (NPs, around 55 nm, citrate-stabilized method[20]) on the polycrystalline Au-coated film (Angstrom Engineering, 99.999% purity). The NP cast Au film was then transferred into the 50 mM H_2SO_4 solution for voltammetric cleaning (scanned from 1.3 to −0.2 V vs Ag/AgCl at 50 mV/s for over 20 min).

Preparation of PyNHC-SAM on a Au Substrate (SERS). The PyNHC-SAM on a Au substrate was prepared by soaking the pre-made Au SERS-active film into the 5 mg/mL $[(PyNHC)_2Au]PF_6$ ethanol solution overnight at open-circuit potential.

Preparation of PyNHC-SAM on a Au Substrate (PM-IRRAS and XPS). For PM-IRRAS studies as well as XPS characterization, monolayers were prepared by soaking a piranha-etched Au-coated glass slide in a 1 mg/mL solution of $[(PyNHC)_2Au]PF_6$ in ethanol overnight. The following day the slides were rinsed heavily with 1 M aqueous NaOH, distilled water, ethanol, and dichloromethane (DCM) sequentially and sonicated briefly (30 s to 1 min) in DCM solution to remove any residual physiosorbed material. The slides were then dried under a stream of nitrogen prior to PM-IRRAS measurements.

https://doi.org/10.1021/jacs.3c14113
J. Am. Chem. Soc. 2024, 146, 10489−10497

Scheme 2. Synthetic Route to the Studied Monolayer Precursor $[(PyNHC)_2Au]PF_6$

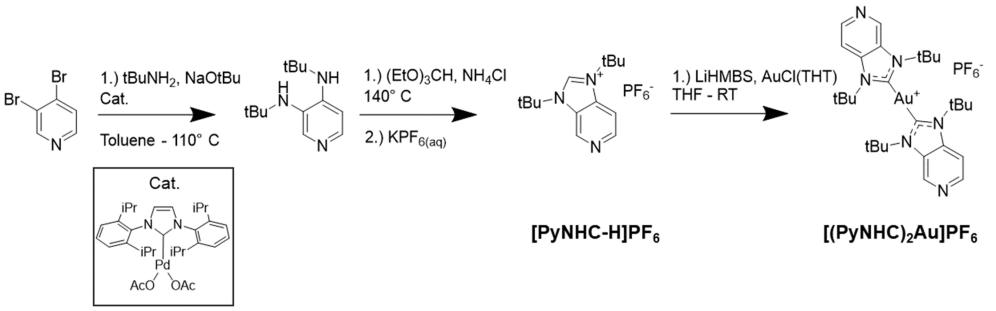

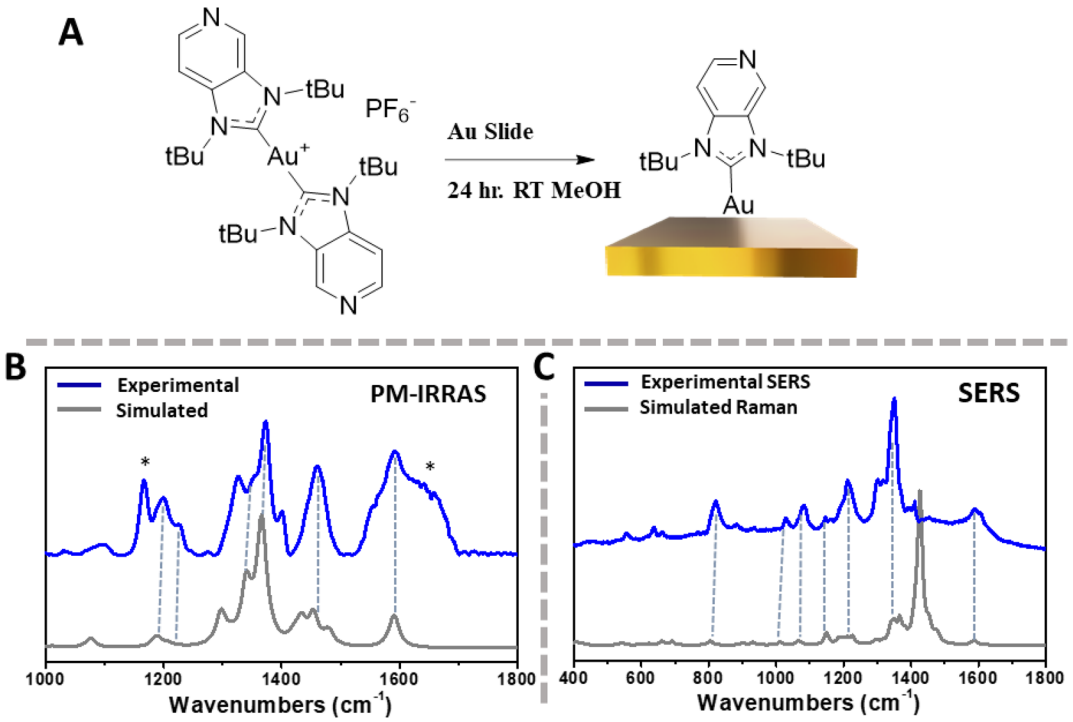

Figure 1. (A) Proposed binding scheme for monolayer formation from $[(PyNHC)_2Au]PF_6$ to form surface-bound PyNHC. (B) PM-IRRAS spectrum of the formed monolayer of PyNHC on a Au-coated glass slide and simulated PM-IRRAS spectra using a DFT cluster model of PyNHC on an Au adatom. (C) SERS spectrum of the formed monolayer of PyNHC and simulated Raman spectrum. For the simulated Raman spectrum, no surface-enhancement effects were considered for the calculated intensities. Peaks marked with an asterisk indicate peaks observed in blank Au slides treated with the same conditions in the absence of $[(PyNHC)_2Au]PF_6$.

Reaction of PyNHC Monolayer with $W(CO)_5THF$. A freshly prepared PyNHC-functionalized Au slide was immersed in a 1 mM solution of $W(CO)_5THF$ for 24 h. The slide was then rinsed heavily with THF and DCM sequentially and sonicated for 30 s in DCM to remove any residual physiosorbed $W(CO)_5THF$ and $W(CO)_6$. The slides were then dried under a stream of dry nitrogen before PM-IRRAS measurements.

Computational Methods. Periodic slab structural models and cluster models were built by DFT geometry optimization of PyNHC binding on Au(111) model surfaces. The low-coordinated environment of Au atoms on cluster edges introduces strong interactions of these boundary atoms with the adsorbed PyNHC molecule. Therefore, the periodic slab models were employed to avoid such effects for investigating PyNHC binding modes as well as benchmark cluster models, while cluster models were utilized for computing free energies and spectra. The binding geometries were investigated after energy minimization of the slab models, using the Vienna Ab Initio Simulation Package (VASP) version 5.4.1,[21−25] with the Perdew−Burke−Ernzerhof (PBE) exchange−correlation functional,[26] Grimme's DFT-D3 dispersion correction (Becke−Johnson damping),[27,28] and the projector-augmented wave (PAW) method with a 450 eV cutoff.[25,29] Binding stability and spectroscopy calculations were performed on cluster models utilizing the Gaussian 16 revision C.01 package,[30] with the ωB97X-D exchange−correction functional,[31] the Def2SVP basis set and effective core potential (ECP)[32] for Au atoms, and the 6-31G(d,p) basis set[33,34] for all other atoms. The PM-IRRAS spectra were calculated from the Gaussian outputs with an in-house custom script. Further details of the computational methods are provided in the SI.

RESULTS AND DISCUSSION

Scheme 2 shows the $[PyNHC-H]^+$ precursor synthesized in a two-step route through a palladium-mediated coupling of 3,4-dibromopyridine with *tert*-butylamine, followed by ring-closing with triethylorthoformate to form the imidazolium salt. The selection of *tert*-butyl groups for the NHC was motivated by their steric bulk, which putatively favors an upright orientation.[35] The 3,4-di(*tert*-butylamino)pyridine was ring-closed to the imidazolium salt via reflux in triethyl orthoformate with a proton source (NH_4Cl), affording $[PyNHC-H]PF_6$ in good yields after ion metathesis with

https://doi.org/10.1021/jacs.3c14113
J. Am. Chem. Soc. 2024, 146, 10489−10497

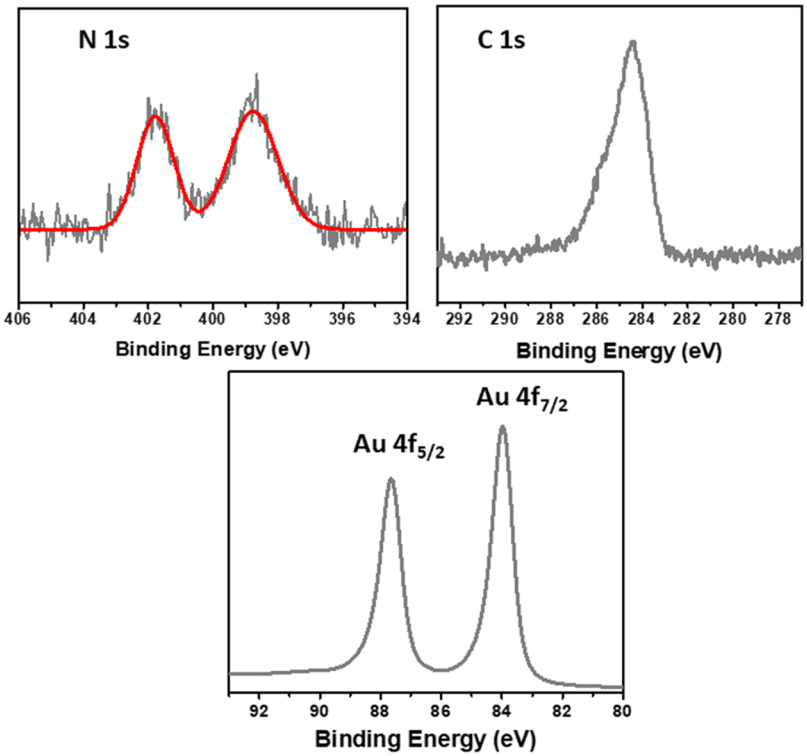

Figure 2. XPS spectra of Au surfaces treated with $[(PyNHC)_2Au]PF_6$ in ethanol solution showing the N 1s, C 1s, and Au 4f regions. Simulated trace of the N 1s region is shown, fitted using two Lorentzian peaks centered at 401.8 and 398.8, respectively.

KPF_6. This salt is bench stable and can be prepared on multigram scales in reasonable yields. The homoleptic gold complex was prepared stepwise in a one-pot protocol by deprotonation of $[PyNHC\text{-}H]PF_6$ using lithium bis-(trimethylsilyl)amide in toluene to generate the free carbene, followed by the addition of tetrahydrothiophene gold(I) chloride, (THT)AuCl. When (THT)AuCl is used as the gold source in a half-equivalent stoichiometry, the reaction favors the formation of the $[(PyNHC)_2Au]^+$ cation over the neutral heteroleptic (PyNHC)AuCl complex, which can be verified by the exclusive observation of the $[(PyNHC)_2Au]^+$ cation at 660.4 m/z in ESI-MS. Extracting the crude product mixture from $KPF_{6(aq)}$ with DCM affords the $[(PyNHC)_2Au]$-PF_6 salt cleanly.

When freshly cleaned Au slides were submerged in dilute (1−5 mg/mL) solutions of $[(PyNHC)_2Au]PF_6$ in ethanol, acetonitrile, or DCM, monolayer formation was observed. We chose to study these monolayers with SERS and PM-IRRAS as complementary surface-sensitive vibrational spectroscopy techniques which could provide structural information about the surface chemistry when cross-referenced against quantum chemical simulations.

Figure 1 shows a schematic of the surface deposition reaction and the resulting SERS and PM-IRRAS spectra of the monolayers. We chose to focus on the analysis of the modes that could be definitively assigned to specific structural features of the SAM since most peaks observed in both the SERS and PM-IRRAS spectra of the PyNHC-SAM are within the fingerprint region which can overlap with atmospheric species, physisorbed solvents, and materials used in the spectroscopic setup. Two examples of this appear in Figure 1B, both of which are marked with an asterisk. The first is a broad mode around ∼1650 cm^{-1} corresponding the H−O bending of adventitious water, and the second is a sharp feature at ∼1150 corresponding to the Si−O stretch of the glass slide. The first, most intense and sharp peak corresponding to PyNHC in the PM-IRRAS spectra is centered at 1373 cm^{-1}. This feature can be assigned to a localized C−N stretching mode of the NHC moiety predominantly centered at the displacement of the carbene atom. The second peak is the pyridine ring C═C/C═N stretching mode at 1593 cm^{-1} that is present and resolvable in both the PM-IRRAS and SERS spectra. In the PM-IRRAS, the 1593 cm^{-1} stretch overlaps with the broad H−O−H bend of adventitious water, which we were not capable of removing from the sample even with diligent drying measures, suggesting a hygroscopic nature of this SAM.

To obtain a detailed understanding of the observed PM-IRRAS and SERS spectra, we performed DFT calculations of the vibrational spectrum of Au-bound PyNHC using a cluster-based model (see the Methods and SI). The calculated PM-IRRAS largely agrees with the experimental frequencies and intensities, suggesting that the binding mode of the NHC in the computational structural model is an accurate representation of the behavior of the monolayer under ambient conditions. A simulated flat-lying geometry results in a spectrum with a lower intensity of the 1373 cm^{-1} C−N stretching mode, due to the mode lying more parallel to the reflection surface (Figure S4). Parallel-oriented modes have minimal intensity by the PM-IRRAS selection rules, which only enhance vibrational modes with transition dipoles normal to the reflection plane.[36] The observed spectrum showcasing the 1373 cm^{-1} peak as the most intense suggests that the upright orientation is the preferred binding mode. Our results further support previous findings that suggest that NHCs with large R groups prefer an upright orientation.[4] The calculated Raman frequencies also agree with the observed vibrational frequencies, although the SERS technique results in dramatic enhancement of the intensities of certain peaks within the

https://doi.org/10.1021/jacs.3c14113
J. Am. Chem. Soc. 2024, 146, 10489−10497

Raman spectra.[37] An example of this is in a mode centered at 1426 cm^{-1} in the simulated Raman spectrum, which corresponds to a C−H bend on the *t*-Bu groups. This mode is the most intense in the simulated Raman spectra, but is dwarfed by the 1346 cm^{-1} C−N stretch in the experimental spectrum. This is likely a result of surface enhancement of modes with polarizability and dipole moments normal and proximal to the Au surface excluding the C−H bending mode which is predominantly parallel to the proposed binding geometry and would be minimally enhanced by both chemical and electromagnetic SERS enhancement mechanisms.

To corroborate our vibrational characterization of these monolayers with previous literature reports on NHC-based monolayers, we examined the prepared surfaces using XPS. Figure 2 shows the C 1s, N 1s, and Au 4f regions of the collected XPS spectrum. The N 1s region of the XPS spectrum displays two features. The first feature at a binding energy of 401.8 eV mirrors previous characterizations of NHC-based monolayers corresponding to the nitrogen atoms in the imidazole ring. In this case the N (1s) peak shows a slightly higher binding energy corresponding to the more electron deficient imidazopyridine heterocycle compared to imidazole- and benzimidazole-derived NHCs reported elsewhere.[5,7,13] The second N 1s feature occurs at 398.8, corresponding to the pyridinic nitrogen, in good agreement with previously reported thiol-anchored alkylpyridine-based monolayers.[38,39] We found a N/Au atom ratio of 0.07:1, which corresponds to monolayer/submonolayer surface coverages reported previously.[40] We also observed a F (1s) signal in the XPS survey sweep with a N/F ratio of 0.68:1, corresponding to an NHC/PF_6 ratio of 1.36:1. While lower than the 2:1 ratio expected from the parent molecule, this suggests a substantial retention of positive surface charge at gold. This is further supported by a detailed charge analysis of density functional theory models, which demonstrate the surface-bound adatoms retain a partial positive charge relative to the bulk gold These results and discussion are included in the SI of this article (Table S-1). Whether this positive surface charge is originally derived from our oxidative cleaning protocol of the gold slides or is a result of the reaction between the presumably neutral bulk gold and the $NHC_2Au(I)$ fragment is still unclear. The charge behavior of these NHC-bound adatoms could provide an intermediate chemical environment that may bridge the gaps between the discrete reductions and oxidations of homogeneous metal complexes with the continuous charging behavior of bulk metallic surfaces and is an area of great interest to us.

The mechanism of the observed monolayer formation is not entirely understood, although several formation schemes can be considered for the observed surface deposition. Cationic gold NHC complexes have frequently been used as molecular precursors for nanoparticle synthesis, requiring a reductant such as $NaBH_4$ to nucleate the growth of metallic gold from the Au(I) precursors.[11] Electrons originating from the bulk gold surface could act as reducing equivalents to allow for the deposition of the Au(I) atom. While thermally stable, homoleptic gold NHC complexes have been known to undergo ligand scrambling reactions.[13,41,42] Whether cationic bis-NHC gold complexes are deposited through a redox process or simply transferred to the surface in a "ligand exchange" is a question well worth answering. However, we have unfortunately not been able to address this using conventional surface characterization techniques.

To further investigate the binding mode and the orientation of PyNHC on the surface, we investigated the binding mode of PyNHC by employing DFT calculations of both Au slabs and cluster models. The free carbene, when directly bound to the slab surface, displaces the bound Au atom from the surface (Figure 3B) due to the steric bulk of the *t*-Bu groups. Several

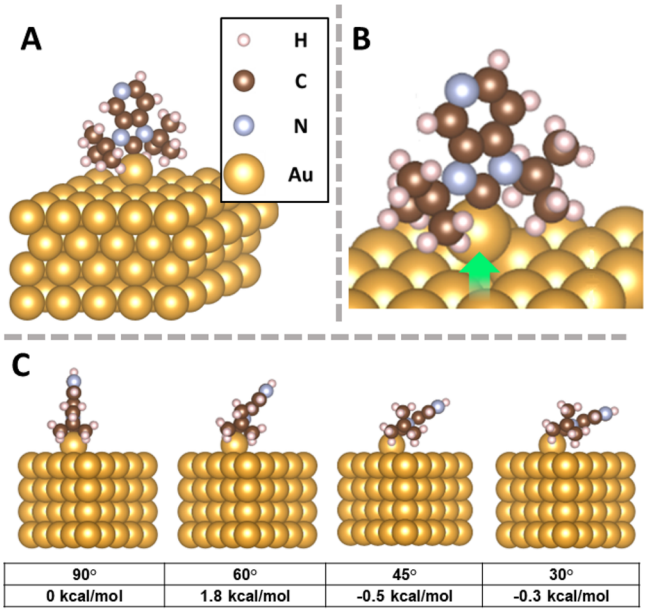

Figure 3. (A) Calculated binding geometry of PyNHC atop an adatom on a Au(111) slab. (B) Resulting optimized geometry of the reaction of free NHC with a flat Au(111) surface without an adatom showcasing the abstraction of a gold atom from the surface. (C) Optimized structures and relative energies of different tilt angles of adatom-bound PyNHC showcasing the low barriers to tilting.

reports have found that this adatom binding mode is quite mobile, frequently being likened to a "ballbot" which can roll across a flat Au(111) surface with minimal barriers.[43] This dynamic chemistry has already proven useful when trying to facilitate surface-anchored reactivity[44] and likely plays a role in allowing NHC-based monolayers to form such well-ordered domains. We further investigated the energy landscape of the adatom binding geometry of the PyNHC. Azimuthal rotation of the PyNHC by 90° does not change the electronic energy of the system. Tilting the PyNHC from the vertical (90°) to a 30° binding angle also produces minimal changes in energy (Figure 3C). This suggests that PyNHC can rotate and reorient rapidly under standard conditions; therefore, the preferred azimuthal orientation must result from monolayer packing and discrete solvent interactions. The thermodynamically favorable flat orientation reported in a previous work[45] is likely due to the preferential interaction between the NHC ligand and low-coordinated Au atoms, mostly on cluster edges.

We have also investigated the stability of the PyNHC adatom on the gold surface as described at the DFT level of theory, using a cluster model structure in an implicit solvent modeling acetonitrile by the polarizable continuum model (PCM).[46] The Au(111) surface is represented by a 21-atom cluster containing two layers. The binding energy was simulated using the reaction schematically represented in Figure 4, in which [(PyNHC)Au]-L binds to a planar Au surface together with the Au adatom to generate a net positive surface charge, releasing one equivalent of ligand L. The

https://doi.org/10.1021/jacs.3c14113
J. Am. Chem. Soc. 2024, 146, 10489−10497

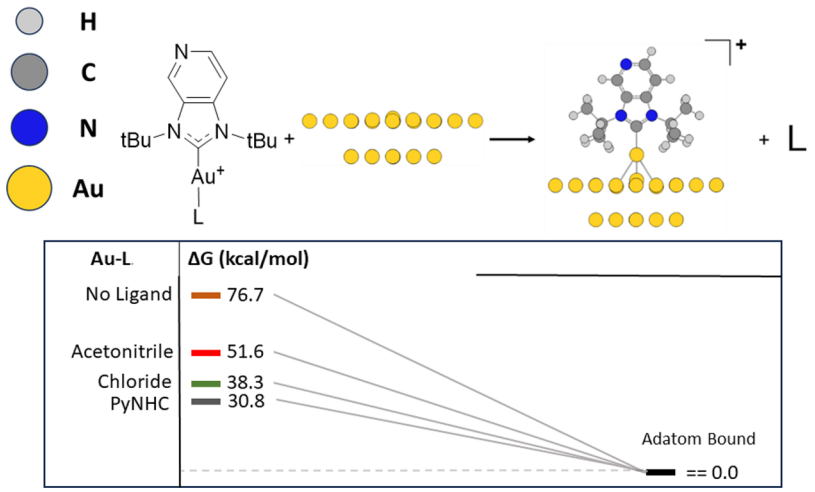

Figure 4. (Top) Representation of the simulated (PyNHC)Au-L binding reaction to the gold surface in acetonitrile. (Bottom) Gibbs free energy of various (PyNHC)Au-L species relative to the surface-bound PyNHC. "No Ligand" refers to $[(PyNHC)Au]^+$; PyNHC refers to $[(PyNHC)_2Au]^+$. L refers to the products of a ligand disassociation, with acetonitrile and PyNHC leaving as neutral ligands and chloride leaving as an anion.

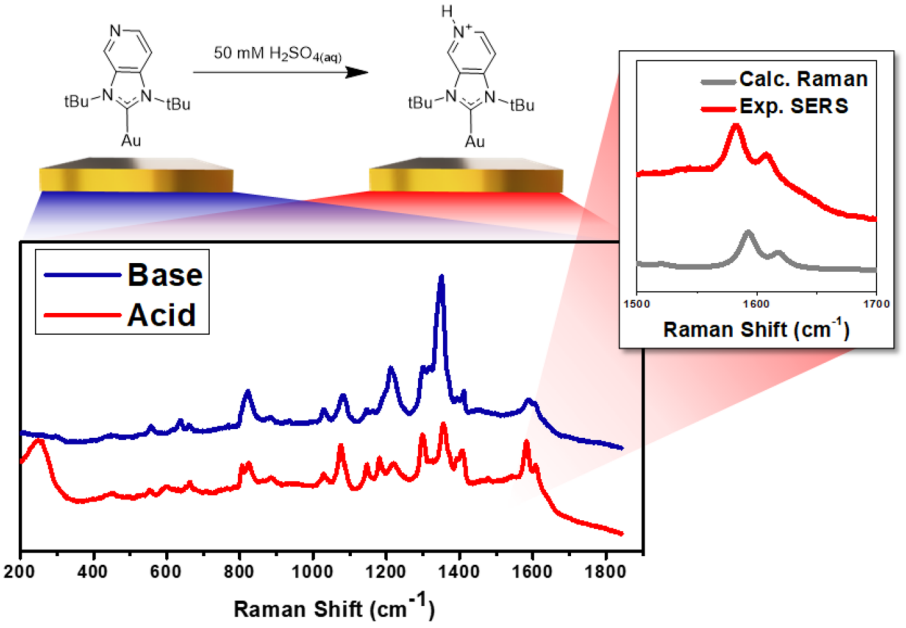

Figure 5. Schematic for the protonation of PyNHC monolayers with H_2SO_4 (top left) SERS spectra in the double-bond region of monolayers of PyNHC before (blue) and after treatment with $H_2SO_{4(aq)}$ (red) and inset comparing the 1500−1700 cm^1 region of the experimental SERS with simulated Raman intensities of the protonated species (gray).

binding energies of [(PyNHC)Au]-L with different ligands (L) are displayed in the bottom half of Figure 4. Chloride, acetonitrile, and PyNHC were chosen, as they represent experimentally observed homogeneous complexes, suggesting they are the most stable homogeneous species to compare with the proposed binding mode. The studied ligands favor the surface-bound geometry over the molecular gold complexes. Experimentally, the monolayers are still stable under a strong aqueous base (1 M NaOH). Considering the small electronic energy change ΔE = 1.8 kcal/mol corresponding to a free energy change of 6.1 kcal/mol for this reaction (1.0 and 5.2 kcal/mol in the PCM implicit water solvent, correspondingly), the discrepancy between the computational and experimental results likely originates from the approximate representation of the Au surface. Binding of the synthesized homoleptic complex (and release of a PyNHC carbene) is an exothermic, spontaneous reaction (ΔE = −30.8 kcal/mol, corresponding to ΔE = −30.8 kcal/mol). The binding reactions with chloride and acetonitrile are even more favorable, with Gibbs free energy changes of −38.3 and −51.6 kcal/mol, respectively, indicating that neither strongly coordinating anions nor organic solvents destabilize the Au-bound PyNHC monolayers. This is anecdotally supported by the observation that only a 3:1 prepared piranha solution is adequate to properly clean the Au slides after monolayer deposition.

We investigated the stability of the monolayers under strong acidic conditions to further verify that the surface deposition method resulted in the formation of an NHC-centered surface attachment. Previously NHC-based monolayers have been found to be extraordinarily stable under harshly acidic conditions.[5]

https://doi.org/10.1021/jacs.3c14113
J. Am. Chem. Soc. 2024, 146, 10489−10497

Figure 5 shows the result of treating monolayers of PyNHC with 50 mM aqueous sulfuric acid. In the SERS spectra of acid-treated monolayers, the pyridine C═C stretch at 1593 cm^{-1} shifts to higher frequency, and an additional feature appears. Upon comparison with the cluster model simulations, we find good agreement with the computed Raman spectrum for protonated H^+-PyNHC, including the observation of an additional mode in the 1500−1700 cm^{-1} region, corresponding to a N−H bending mode (Figure S3). Additionally, when acid-treated monolayers were treated with a 1 M sodium hydroxide solution, the SERS spectra reverted, regenerating the SERS response initially recorded (Figure S5). In PM-IRRAS, the overlap of those modes with the H−O−H bending mode of adventitious water precluded confident analysis of the peaks. Similarly, significant broadening in the N−H stretching region around 3500 cm^{-1} prevented any substantive analysis of the protonation equilibrium. However, PM-IRRAS was useful for verifying the bulk stability of the monolayers under acidic conditions, with no substantial loss of signal when immersed in acidic solutions of 5 M $H_2SO_{4(aq)}$ for 1 h (Figure S-8). These experiments verified that our monolayer preparation successfully results in strong chemical surface attachment, as reported previously, and demonstrates the retention of acid−base reactivity of the pyridine functional groups at the interface.

Finally, we are interested in utilizing monolayers to scaffold the formation of transition metal complexes on metallic gold surfaces. To provide a proof-of-concept for how these pyridine-functionalized monolayers could be used, we chose to react the PyNHC monolayers with a transition metal carbonyl species. $W(CO)_5(THF)$ readily undergoes ligand exchange with the weakly coordinating THF solvate and has very intense vibrational modes corresponding to the ν(CO) stretches of the substituted tungsten pentacarbonyl. We had initially attempted this reaction with the homoleptic gold precursor to generate a $[(W(CO)_5PyNHC)_2Au]PF_6$ complex. Unfortunately, the addition of the $W(CO)_5$ moiety made the product too photosensitive to confidently isolate, although the species could be observed in situ by an FTIR spectrum, which agrees with a $W(CO)_5$pyridine-type complex. The photodegradation coincided with the formation of a metallic gold precipitate, likely stemming from the reduction of the NHC_2Au^+ cation.[11] This loosely demonstrates that the NHC_2Au^+ cations can act as foundations for constructing more elaborate bottom-up assemblies for subsequent surface attachment. A less photoactive species would prove to be a more robust demonstration of this approach. Due to the instability of the homogeneous species, a stepwise approach was taken to first form monolayers of PyNHC, followed by treatment of those monolayers with a freshly prepared solution of 1 mM $W(CO)_5(THF)$ in THF and then by vigorous washing and sonication in DCM to ensure the complete removal of physisorbed $W(CO)_5THF$. Figure 6 shows the PM-IRRAS spectra before and after the treatment of PyNHC-SAM with THF solutions of $W(CO)_5THF$. The ν(CO) region of the PM-IRRAS after the reaction reveals four new peaks, with two weak features at 2069 and 1977 cm^{-1}, a very sharp and intense peak at 1926 cm^{-1}, and a shoulder centered at 1893 cm^{-1}, closely agreeing with the literature values for N-coordinated tungsten pentacarbonyl complexes.[47] While this work demonstrates the ability to introduce NHC-attached metal carbonyls to a gold surface, it also presents a proof-of-concept showing that we can conduct stepwise on-surface reactions with the pyridine acting as a ligand.

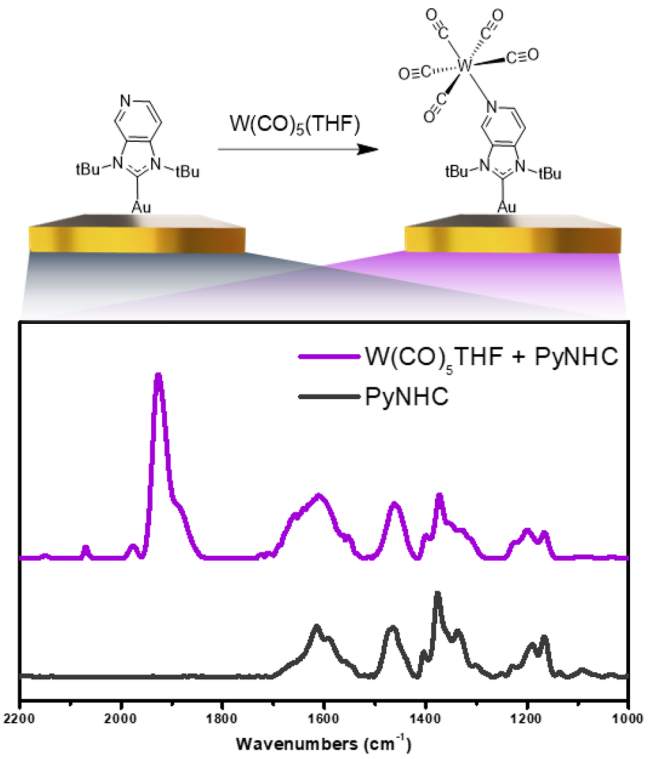

Figure 6. Schematic for the ligand exchange reaction of the PyNHC monolayer with $W(CO)_5(THF)$ and the PM-IRRAS spectrum before (black) and after the reaction with $W(CO)_5THF$ (purple).

CONCLUSIONS

We have demonstrated a means of constructing NHC-anchored monolayers bearing a pyridine moiety. We have analyzed the binding mode of the PyNHC monolayer at the DFT level, allowing us to calculate vibrational spectra, providing an understanding of the PM-IRRAS, SERS, and XPS experimental data, including information on the surface-binding orientation under ambient conditions. The DFT analysis also provides the thermodynamic landscape of surface binding in the presence of competitive coordinating solvents and ions and verified that landscape with experimental observations of the SAM's stability. We found that the PyNHC-SAMs can act as both Lewis and Bronsted bases and are experimentally observable in protonated and deprotonated states. This reactivity could be useful in determining the influence of interfaces on the pK_a of surface-bound molecules. We also demonstrate that PyNHC SAMs undergo ligand substitution reactions with $W(CO)_5THF$ to generate surface-bound organometallic species that act as strong vibrational chromophores. This provides precedence for conducting bottom-up synthesis of transition metal species starting from NHC-SAMs acting as ligands, which could be useful reactivity for tailoring metal and semimetal interfaces for both single molecule and bulk electronic devices, chemical sensors, biotechnology, and catalysts.

ASSOCIATED CONTENT

Supporting Information

The Supporting Information is available free of charge at https://pubs.acs.org/doi/10.1021/jacs.3c14113.

Synthetic procedures and additional homogeneous characterization, PM-IRRAS, SERS and XPS exper-

https://doi.org/10.1021/jacs.3c14113
J. Am. Chem. Soc. 2024, 146, 10489−10497

imental collection and analysis parameters, computational details, methodology and further data analysis, and supplemental figures (PDF)

AUTHOR INFORMATION

Corresponding Author

Clifford P. Kubiak − *Department of Chemistry and Biochemistry, University of California, San Diego, La Jolla, California 92093, United States;* orcid.org/0000-0003-2186-488X; Email: ckubiak@ucsd.edu

Authors

Joseph M. Palasz − *Department of Chemistry and Biochemistry, University of California, San Diego, La Jolla, California 92093, United States*

Zhuoran Long − *Department of Chemistry and Energy Sciences Institute, Yale University, New Haven, Connecticut 06520, United States;* orcid.org/0000-0002-2957-9568

Jinhui Meng − *Department of Chemistry, Emory University, Atlanta, Georgia 30322, United States*

Pablo E. Videla − *Department of Chemistry and Energy Sciences Institute, Yale University, New Haven, Connecticut 06520, United States;* orcid.org/0000-0003-0742-0342

H. Ray Kelly − *Department of Chemistry and Energy Sciences Institute, Yale University, New Haven, Connecticut 06520, United States;* orcid.org/0000-0003-3811-0662

Tianquan Lian − *Department of Chemistry, Emory University, Atlanta, Georgia 30322, United States;* orcid.org/0000-0002-8351-3690

Victor S. Batista − *Department of Chemistry and Energy Sciences Institute, Yale University, New Haven, Connecticut 06520, United States;* orcid.org/0000-0002-3262-1237

Complete contact information is available at: https://pubs.acs.org/10.1021/jacs.3c14113

Author Contributions

#J.M.P. and Z.L. contributed equally to this work.

Notes

The authors declare no competing financial interest.

ACKNOWLEDGMENTS

C.P.K. and J.M.P. gratefully acknowledge financial support from NSF (CHE-1853908 and CHE-2153757). The work was partially supported by AFOSR grant FA9550-17-0198 (V.S.B., T.L., and C.P.K.) and by U.S. Army Research Office Award W911NF2110337 (V.S.B.). The *in situ* surface-enhanced Raman measurements are supported by the Air Force Office of Scientific Research under award number FA9550-18-1-0420 (J.M., T.L.). Z.L., P.E.V., H.R.K., and V.S.B. gratefully acknowledge the computation resources from the Yale Center for Research Computing and the National Energy Research Scientific Computing Center (NERSC), a U.S. Department of Energy Office of Science User Facility at Lawrence Berkeley National Laboratory. The authors thank James Taylor for their invaluable assistance preparing the revised manuscript. We must also thank Thomas Chan and Rajiv Prabhakar at Lawrence Berkeley National Laboratory for their assistance in acquiring XPS characterization of our materials.

REFERENCES

(1) Ulman, A. Formation and Structure of Self-Assembled Monolayers. *Chem. Rev.* **1996**, *96* (4), 1533−1554.

(2) Vericat, C.; Vela, M. E.; Benitez, G.; Carro, P.; Salvarezza, R. C. Self-assembled monolayers of thiols and dithiols on gold: new challenges for a well-known system. *Chem. Soc. Rev.* **2010**, *39* (5), 1805−1834.

(3) Larrea, C. R.; Baddeley, C. J.; Narouz, M. R.; Mosey, N. J.; Horton, J. H.; Crudden, C. M. N-Heterocyclic Carbene Self-assembled Monolayers on Copper and Gold: Dramatic Effect of Wingtip Groups on Binding, Orientation and Assembly. *ChemPhysChem* **2017**, *18* (24), 3536−3539.

(4) Inayeh, A.; Groome, R. R. K.; Singh, I.; Veinot, A. J.; de Lima, F. C.; Miwa, R. H.; Crudden, C. M.; McLean, A. B. Self-assembly of N-heterocyclic carbenes on Au(111). *Nat. Commun.* **2021**, *12* (1), 4034.

(5) Crudden, C. M.; Horton, J. H.; Ebralidze, I. I.; Zenkina, O. V.; McLean, A. B.; Drevniok, B.; She, Z.; Kraatz, H.-B.; Mosey, N. J.; Seki, T.; Keske, E. C.; Leake, J. D.; Rousina-Webb, A.; Wu, G. Ultra stable self-assembled monolayers of N-heterocyclic carbenes on gold. *Nat. Chem.* **2014**, *6* (5), 409−414.

(6) Amit, E.; Dery, L.; Dery, S.; Kim, S.; Roy, A.; Hu, Q.; Gutkin, V.; Eisenberg, H.; Stein, T.; Mandler, D.; Dean Toste, F.; Gross, E. Electrochemical deposition of N-heterocyclic carbene monolayers on metal surfaces. *Nat. Commun.* **2020**, *11* (1), 5714.

(7) Crudden, C. M.; Horton, J. H.; Narouz, M. R.; Li, Z.; Smith, C. A.; Munro, K.; Baddeley, C. J.; Larrea, C. R.; Drevniok, B.; Thanabalasingam, B.; McLean, A. B.; Zenkina, O. V.; Ebralidze, I. I.; She, Z.; Kraatz, H.-B.; Mosey, N. J.; Saunders, L. N.; Yagi, A. Simple direct formation of self-assembled N-heterocyclic carbene monolayers on gold and their application in biosensing. *Nat. Commun.* **2016**, *7* (1), 12654.

(8) Angove, E.; Grillo, F.; Früchtl, H. A.; Veinot, A. J.; Singh, I.; Horton, J. H.; Crudden, C. M.; Baddeley, C. J. Highly Ordered N-Heterocyclic Carbene Monolayers on Cu(111). *J. Phys. Chem. Lett.* **2022**, *13* (8), 2051−2056.

(9) DeJesus, J. F.; Trujillo, M. J.; Camden, J. P.; Jenkins, D. M. N-Heterocyclic Carbenes as a Robust Platform for Surface-Enhanced Raman Spectroscopy. *J. Am. Chem. Soc.* **2018**, *140* (4), 1247−1250.

(10) Fèvre, M.; Pinaud, J.; Leteneur, A.; Gnanou, Y.; Vignolle, J.; Taton, D.; Miqueu, K.; Sotiropoulos, J.-M. Imidazol(in)ium Hydrogen Carbonates as a Genuine Source of N-Heterocyclic Carbenes (NHCs): Applications to the Facile Preparation of NHC Metal Complexes and to NHC-Organocatalyzed Molecular and Macromolecular Syntheses. *J. Am. Chem. Soc.* **2012**, *134* (15), 6776−6784.

(11) Vignolle, J.; Tilley, T. D. N-Heterocyclic carbene-stabilized gold nanoparticles and their assembly into 3D superlattices. *Chem. Commun.* **2009**, No. 46, 7230−7232.

(12) Doud, E. A.; Inkpen, M. S.; Lovat, G.; Montes, E.; Paley, D. W.; Steigerwald, M. L.; Vázquez, H.; Venkataraman, L.; Roy, X. In Situ Formation of N-Heterocyclic Carbene-Bound Single-Molecule Junctions. *J. Am. Chem. Soc.* **2018**, *140* (28), 8944−8949.

(13) DeJesus, J. F.; Sherman, L. M.; Yohannan, D. J.; Becca, J. C.; Strausser, S. L.; Karger, L. F. P.; Jensen, L.; Jenkins, D. M.; Camden, J. P. A Benchtop Method for Appending Protic Functional Groups to N-Heterocyclic Carbene Protected Gold Nanoparticles. *Angew. Chem., Int. Ed.* **2020**, *59* (19), 7585−7590.

(14) MacLeod, M. J.; Goodman, A. J.; Ye, H.-Z.; Nguyen, H. V. T.; Van Voorhis, T.; Johnson, J. A. Robust gold nanorods stabilized by bidentate N-heterocyclic-carbene−thiolate ligands. *Nat. Chem.* **2019**, *11* (1), 57−63.

(15) Salorinne, K.; Man, R. W. Y.; Li, C.-H.; Taki, M.; Nambo, M.; Crudden, C. M. Water-Soluble N-Heterocyclic Carbene-Protected Gold Nanoparticles: Size-Controlled Synthesis, Stability, and Optical Properties. *Angew. Chem., Int. Ed.* **2017**, *56* (22), 6198−6202.

(16) Bridonneau, N.; Hippolyte, L.; Mercier, D.; Portehault, D.; Desage-El Murr, M.; Marcus, P.; Fensterbank, L.; Chanéac, C.; Ribot, F. N-Heterocyclic carbene-stabilized gold nanoparticles with tunable sizes. *Dalton Trans.* **2018**, *47* (19), 6850−6859.

(17) Stolz, I. W.; Haas, H.; Sheline, R. K. Infrared Spectroscopic Evidence for New Metal Carbonyl Complexes with Aromatic Ligands. *J. Am. Chem. Soc.* **1965**, *87* (4), 716−718.

(18) Ullah, F.; Shanmuganathan, S.; Schindler, C.; Jones, P. G.; Heinicke, J. W. Influence of pyrido-annulation on N,N′-dineopentylimidazolin-2-ylidene and associated transition metal complexes; comparison with benzo-, naphtho- and quinoxalino-annulation. *J. Organomet. Chem.* **2019**, *890*, 43−57.
(19) Baker, M. V.; Barnard, P. J.; Berners-Price, S. J.; Brayshaw, S. K.; Hickey, J. L.; Skelton, B. W.; White, A. H. Cationic, linear Au(i) N-heterocyclic carbene complexes: synthesis, structure and anti-mitochondrial activity. *Dalton Trans.* **2006**, No. 30, 3708.
(20) Li, J. F.; Huang, Y. F.; Ding, Y.; Yang, Z. L.; Li, S. B.; Zhou, X. S.; Fan, F. R.; Zhang, W.; Zhou, Z. Y.; Wu, D. Y.; Ren, B.; Wang, Z. L.; Tian, Z. Q. Shell-isolated nanoparticle-enhanced Raman spectroscopy. *Nature* **2010**, *464* (7287), 392−395.
(21) Kresse, G.; Furthmüller, J. Efficiency of ab-initio total energy calculations for metals and semiconductors using a plane-wave basis set. *Comput. Mater. Sci.* **1996**, *6* (1), 15−50.
(22) Kresse, G.; Furthmüller, J. Efficient iterative schemes for ab initio total-energy calculations using a plane-wave basis set. *Phys. Rev. B* **1996**, *54* (16), 11169−11186.
(23) Kresse, G.; Hafner, J. Ab initio molecular dynamics for liquid metals. *Phys. Rev. B* **1993**, *47* (1), 558−561.
(24) Kresse, G.; Hafner, J. Ab initio molecular-dynamics simulation of the liquid-metal–amorphous-semiconductor transition in germanium. *Phys. Rev. B* **1994**, *49* (20), 14251−14269.
(25) Kresse, G.; Joubert, D. From ultrasoft pseudopotentials to the projector augmented-wave method. *Phys. Rev. B* **1999**, *59* (3), 1758−1775.
(26) Perdew, J. P.; Burke, K.; Ernzerhof, M. Generalized Gradient Approximation Made Simple. *Phys. Rev. Lett.* **1996**, *77* (18), 3865−3868.
(27) Grimme, S.; Antony, J.; Ehrlich, S.; Krieg, H. A consistent and accurate ab initio parametrization of density functional dispersion correction (DFT-D) for the 94 elements H-Pu. *J. Chem. Phys.* **2010**, *132* (15), 1−19.
(28) Grimme, S.; Ehrlich, S.; Goerigk, L. Effect of the damping function in dispersion corrected density functional theory. *J. Comput. Chem.* **2011**, *32* (7), 1456−1465.
(29) Blöchl, P. E. Projector augmented-wave method. *Phys. Rev. B* **1994**, *50* (24), 17953−17979.
(30) Frisch, M.; Trucks, G.; Schlegel, H. B.; Scuseria, G.; Robb, M.; Cheeseman, J.; Scalmani, G.; Barone, V.; Petersson, G.; Nakatsuji, H.; et al. *Gaussian 16*, Rev. C.01; Gaussian, Inc.: Wallingford, CT, 2016.
(31) Chai, J.-D.; Head-Gordon, M. Long-range corrected hybrid density functionals with damped atom−atom dispersion corrections. *Phys. Chem. Chem. Phys.* **2008**, *10* (44), 6615−6620.
(32) Weigend, F. Accurate Coulomb-fitting basis sets for H to Rn. *Phys. Chem. Chem. Phys.* **2006**, *8* (9), 1057−1065.
(33) Francl, M. M.; Pietro, W. J.; Hehre, W. J.; Binkley, J. S.; Gordon, M. S.; DeFrees, D. J.; Pople, J. A. Self-consistent molecular orbital methods. XXIII. A polarization-type basis set for second-row elements. *J. Chem. Phys.* **1982**, *77* (7), 3654−3665.
(34) Hariharan, P. C.; Pople, J. A. The influence of polarization functions on molecular orbital hydrogenation energies. *Theor. Chim. Acta* **1973**, *28* (3), 213−222.
(35) Ruiz-Castillo, P.; Buchwald, S. L. Applications of Palladium-Catalyzed C−N Cross-Coupling Reactions. *Chem. Rev.* **2016**, *116* (19), 12564−12649.
(36) Zamlynny, V.; Lipkowski, J. Quantitative SNIFTIRS and PM IRRAS of Organic Molecules at Electrode Surfaces. *Adv. Electrochem. Sci. Eng.* **2006**, *9*, 315−376.
(37) Langer, J.; Jimenez de Aberasturi, D.; Aizpurua, J.; Alvarez-Puebla, R. A.; Auguié, B.; Baumberg, J. J.; Bazan, G. C.; Bell, S. E. J.; Boisen, A.; Brolo, A. G.; Choo, J.; Cialla-May, D.; Deckert, V.; Fabris, L.; Faulds, K.; García de Abajo, F. J.; Goodacre, R.; Graham, D.; Haes, A. J.; Haynes, C. L.; Huck, C.; Itoh, T.; Käll, M.; Kneipp, J.; Kotov, N. A.; Kuang, H.; Le Ru, E. C.; Lee, H. K.; Li, J.-F.; Ling, X. Y.; Maier, S. A.; Mayerhöfer, T.; Moskovits, M.; Murakoshi, K.; Nam, J.-M.; Nie, S.; Ozaki, Y.; Pastoriza-Santos, I.; Perez-Juste, J.; Popp, J.; Pucci, A.; Reich, S.; Ren, B.; Schatz, G. C.; Shegai, T.; Schlücker, S.; Tay, L.-L.; Thomas, K. G.; Tian, Z.-Q.; Van Duyne, R. P.; Vo-Dinh, T.; Wang, Y.; Willets, K. A.; Xu, C.; Xu, H.; Xu, Y.; Yamamoto, Y. S.; Zhao, B.; Liz-Marzán, L. M. Present and Future of Surface-Enhanced Raman Scattering. *ACS Nano* **2020**, *14* (1), 28−117.
(38) Liu, J.; Schüpbach, B.; Bashir, A.; Shekhah, O.; Nefedov, A.; Kind, M.; Terfort, A.; Wöll, C. Structural characterization of self-assembled monolayers of pyridine-terminated thiolates on gold. *Phys. Chem. Chem. Phys.* **2010**, *12* (17), 4459−4472.
(39) Ramírez, E. A.; Cortés, E.; Rubert, A. A.; Carro, P.; Benítez, G.; Vela, M. E.; Salvarezza, R. C. Complex Surface Chemistry of 4-Mercaptopyridine Self-Assembled Monolayers on Au(111). *Langmuir* **2012**, *28* (17), 6839−6847.
(40) Pellitero, M. A.; Jensen, I. M.; Dominique, N. L.; Ekowo, L. C.; Camden, J. P.; Jenkins, D. M.; Arroyo-Currás, N. Stability of N-Heterocyclic Carbene Monolayers under Continuous Voltammetric Interrogation. *ACS Appl. Mater. Interfaces* **2023**, *15* (29), 35701−35709.
(41) Goetzfried, S. K.; Gallati, C. M.; Cziferszky, M.; Talmazan, R. A.; Wurst, K.; Liedl, K. R.; Podewitz, M.; Gust, R. N-Heterocyclic Carbene Gold(I) Complexes: Mechanism of the Ligand Scrambling Reaction and Their Oxidation to Gold(III) in Aqueous Solutions. *Inorg. Chem.* **2020**, *59* (20), 15312−15323.
(42) Dos Santos, H. F.; Vieira, M. A.; Sánchez Delgado, G. Y.; Paschoal, D. Ligand Exchange Reaction of Au(I) R-N-Heterocyclic Carbene Complexes with Cysteine. *J. Phys. Chem. A* **2016**, *120* (14), 2250−2259.
(43) Wang, G.; Rühling, A.; Amirjalayer, S.; Knor, M.; Ernst, J. B.; Richter, C.; Gao, H.-J.; Timmer, A.; Gao, H.-Y.; Doltsinis, N. L.; Glorius, F.; Fuchs, H. Ballbot-type motion of N-heterocyclic carbenes on gold surfaces. *Nat. Chem.* **2017**, *9* (2), 152−156.
(44) Ren, J.; Koy, M.; Osthues, H.; Lammers, B. S.; Gutheil, C.; Nyenhuis, M.; Zheng, Q.; Xiao, Y.; Huang, L.; Nalop, A.; Dai, Q.; Gao, H.-J.; Mönig, H.; Doltsinis, N. L.; Fuchs, H.; Glorius, F. On-surface synthesis of ballbot-type N-heterocyclic carbene polymers. *Nat. Chem.* **2023**, *15*, 1737−1744.
(45) Thimes, R. L.; Santos, A. V. B.; Chen, R.; Kaur, G.; Jensen, L.; Jenkins, D. M.; Camden, J. P. Using Surface-Enhanced Raman Spectroscopy to Unravel the Wingtip-Dependent Orientation of N-Heterocyclic Carbenes on Gold Nanoparticles. *J. Phys. Chem. Lett.* **2023**, *14* (18), 4219−4224.
(46) Tomasi, J.; Mennucci, B.; Cammi, R. Quantum Mechanical Continuum Solvation Models. *Chem. Rev.* **2005**, *105* (8), 2999−3094.
(47) Kraihanzel, C. S.; Cotton, F. A. Vibrational Spectra and Bonding in Metal Carbonyls. II. Infrared Spectra of Amine-Substituted Group VI Carbonyls in the CO Stretching Region. *Inorg. Chem.* **1963**, *2* (3), 533−540.

https://doi.org/10.1021/jacs.3c14113
J. Am. Chem. Soc. 2024, 146, 10489−10497